Influence of wavelength and pulse duration on the selective laser ablation of WO_x, VO_x and MoO_x thin films.

C. Munoz-Garcia[1,*], D. Canteli[1], S. Lauzurica[1], M. Morales[1], C. Molpeceres[1], Eloi Ros[2], P. Ortega[2], J.M. López-González[2], C. Voz[2]

[1] Centro Láser. Universidad Politécnica de Madrid (UPM).
C/ Alan Turing 1, 28031, Madrid, Spain
[2] Universitat Politecnica de Catalunya (UPC).
C/ Jordi Girona 1-3, 08034, Barcelona, Spain

[*]Correspondence: cristina.munozg@upm.es

Abstract

In this paper, we present a study of the laser scribing of WO_x, VO_x, and MoO_x films, deposited onto crystalline silicon, with three different wavelengths (355 nm, 532 nm, and 1064 nm) and in two temporal regimes in pulse width, picosecond and nanosecond. For each case, we measure the fluence threshold to remove the transition metal oxides (TMO) film and the fluence threshold to induce damage in the crystalline silicon substrate. The relation between the process parameters and the morphological changes produced in the oxide films is also analysed. The selection of the proper laser source allows a wide parametric window, leading to the complete removal of the TMO films without alteration of the crystalline silicon substrate. Morphological changes of the ablated regions were characterized through confocal microscopy and the relationships between the dimensions of the craters and the ablation parameters were analyzed.

Finally, we present results on the isolation of diodes and their electrical characteristics, showing the quality of the laser scribing processes.

Keywords – transition metal oxides (TMO), hole transport layer, selective contacts, silicon solar cells, laser ablation, fluence threshold.

1. Introduction

The first silicon solar cells presented a high carrier recombination at the silicon wafer surfaces and at the interface between silicon and metal contacts. An early addition was to incorporate a film to passivate the crystalline silicon surface and diminish the charge carrier recombination. Different materials have been used as passivating layers, as SiO_2/SiN_x, Al_2O_3, or amorphous silicon. Specially, amorphous silicon has various advantages: It can be easily doped, the deposition temperatures are very low (below 200ºC) and it has very good passivating properties. This allowed the development of silicon heterojunction solar cells (SHJ) and, shortly after, Heterojunction with Intrinsic Thin Layer (HIT) cells, where a stack of amorphous silicon thin layers (intrinsic and doped) are used to passivate the cell surface and generate the heterojunction [1] [2]. On the other hand, amorphous silicon has the drawback of a very high sheet resistance for the heterojunction emitters [3] [4]. More recently, another passivation alternative proposed is the use of ultrafine SiO_2 combined with a recrystallized phosphorus-doped amorphous silicon layer, named Tunnel Oxide Passivated Contact (TOPcon) [5].

A new promising alternative to a-Si:H in heterojunction solar cells is the use of Transition Metal Oxide (TMO) films as passivating and carrier-selective contacts. These layers are known as selective contacts, i.e., hole or electron transport layers (HTL or ETL, respectively), and can be deposited on both electrodes of a solar cell. In this context, three transition metal oxides, molybdenum oxide (MoO_3), vanadium (V_2O_5) or tungsten (WO_3), acting as front p-type contacts for n-type crystalline silicon heterojunction solar cells have been thoroughly analyzed. The most significant feature of thermally evaporated MoO_x, VO_x and WO_x films is their high chemical potential of up to 6.9 eV, much higher than that of elemental metals. Due to their high working functions (45 eV) and wide energy band gaps, these oxides act as transparent hole-selective contacts with semiconductive properties that are determined by oxygen vacancy defects [6] [7] [8] [9] [10] [11] [12].

Besides adequate materials for the selective contacts, appropriate processing technologies, industrially scalable, to produce final devices is compulsory. In photovoltaics, lasers have become a very powerful, precise, and versatile tool, allowing the improvement of processes as wafer cutting, edge isolation, or surface functionalization, and the development of new others as local doping, laser groove buried contacts, laser-firing contacts, or selective crystallization. Laser scribing, understood as the controlled removal of small volumes of material, has been widely used for the ablation of thin films [13] [14]. One of the more common applications of laser scribing is in the monolithic series-interconnection for thin-film solar panels [15] [16], were different laser processes selectively remove the cell layers to define and interconnect the solar cells [17] [18] [19]. Laser technology also helped the development of interdigitated back-contact cells (IBC), where having both contacts in the back side of the cell allows the use of more transparent antireflective and passivating front layers, along with the reduction of the shadow effect [20] [21] [22].

Laser scribing can be described in a general way as the irradiation of the material surface, leading to the heating, melting, and evaporation of the material. To have a full image of the laser scribing of thin films, we should analyse the main parameters in the process. First, the laser wavelength is going to affect not only the process efficiency but also the possibility to selectively remove the top layer, depending on the absorption coefficients of the top layer and the substrate[23]. The sample structure can affect the result, as the laser light can be mainly absorbed at the surface or inside the sample, leading sometimes to the removal of material via a thermo-mechanic process called induced ablation [24]. Second, laser light, absorbed by the electrons, is transferred to the material lattice as phonons in a picosecond temporal range, so the pulse duration can affect the pulse effect. Laser pulses in the nanosecond and picosecond ranges (pulse duration over ten ps) act as a heating source, but pulses of shorter duration prevent the thermal diffusion, diminishing the thermal effects and leading to a smaller heat-affected zone (HAZ) [25] [26]. Finally, laser pulse fluence is a key to obtain the complete removal of the top layer without affecting the substrate below. Of course, an adequate pulse repetition frequency and pulse overlap are necessary if more than a single pulse is required to process the target area [27] [28]. Different effects have been studied for thin metal, dielectrics, polymers and transparent conductive films as a function of wavelength [29], pulse duration, beam radius [22], number of pulses [30] and pulse repetition rate [31].

So, with a given laser system where the wavelength and pulse duration are fixed, the effects in the material depend on the laser pulse fluence. We can define a damage fluence threshold as the minimum energy density needed to induce visible damage in the film [32]. Similarly, we can define the fluence threshold for the oxide film removal as the minimum energy density needed to completely remove the oxide film and, finally, the fluence threshold for the damage in the silicon substrate will be the minimum energy density to damage the silicon wafer beneath the oxide film. The parametric window of the process, this is, the range of pulse fluence values that allows the oxide film removal without substrate damage, is determined by the latter two thresholds. Using an adoption of the method described by M. Liu [32], the fluence thresholds previously defined can be determined from the relation between pulse fluence and size of the affected area in the sample, as it will be explained below [15] [33] [34] [35].

In this work, we focus on the laser scribing of three TMO films, WO_x, VO_x and MoO_x, with promising properties to be used as selective contacts. These materials have much larger forbidden bandwidths (E_g>3 eV) than crystalline silicon, being possible to remove them by laser without altering the surface of the crystalline silicon, but it is necessary a parametrization of the ablation process in these devices to afterwards adapt their properties to the solar cells. We analyse the interaction between laser pulses with different wavelength -infrared, visible and ultraviolet radiations- and pulse length -nanosecond and picosecond- with the oxide films. We have determined the different fluence thresholds for the oxide film removal, as well as the process parametric windows. The quality of the laser process is demonstrated by the isolation and measure of diodes of the three materials.

2. Material and methods

2.1. Laser sources

To have a full picture of the film scribing process we studied the influence of laser pulse duration and wavelength. In the nanosecond range, we used three different laser sources: Two Nd:VO_4 DPSS sources, one emitting at 355 nm (HIPPO, from Spectra-Physics) and the other emitting at 532 nm (Explorer, from Spectra-Physics), and a Yb fiber laser emitting at 1064 nm (Pulsed Ytterbium Laser, from Wuhan Raycus Laser Technologies). In the picosecond range, we used a Nd:VO_4 DPSS laser source (Lumera Super Rapid-HE), able to emit at the fundamental Nd wavelength and at doubled and tripled frequencies, allowing the use of 1064 nm, 532 nm, and 355 nm in the experiments. All the laser sources work at the TEM_{00} mode. Technical features of the used laser sources are summarised in Table 1. The last row shows the pulse energy range used in each case.

Table 1. Characteristics of the laser sources used in this work, including the range of pulse energies and pulse maximum fluences used in each case.

Laser media	**ns-pulsed**			**ps-pulsed**
	Hippo	**Explorer**	**Raycus**	**Lumera**
Wavelength	355 nm	532 nm	1064 nm	1064 nm / 532 nm / 355 nm
Beam radius ω_0	19 µm	15 µm	20 µm	62 µm / 41 µm / 33 µm
Maximum Fluence	5.24 J/cm^2	4.79 J/cm^2	18.54 J/cm^2	1.55 J/cm^2 (1064 nm) 2.20 J/cm^2 (532 nm) 1.40 J/cm^2 (355 nm)
Average power	5 W (50 kHz)	>2 W (50 kHz)	20 W	18 W (1064 nm) 8 W (532 nm) 4 W (355 nm)
Frecuency	15-300 kHz	20 -150 kHz	20-60 kHz	0-1000 kHz
Pulse duration	<12 ns (50kHz)	< 15 ns (50 kHz)	125 ns (20kHz)	8 ps
Pulse Energy	2.0-22.6 µJ	1.3-14.7 µJ	40.0-118.0 µJ	36.7-93.3/4.0-56.0/2.0-24.0 µJ

2.2. Sample preparation

For the laser ablation experiments, three different oxide thin-films -MoO_x, VO_x, WO_x- were deposited on crystalline silicon substrates. The powdered V_2O_5, MoO_3 and WO_3 precursors were purchased from Sigma Aldrich with more than 99.99% purity. First, polished n-type Si wafers were dipped in dilute hydrofluoric acid (1%) to remove any native silicon oxide from their surface. Then, the different TMO layers were thermally sublimated in vacuum (<10^{-5} mbar) from a tantalum boat. The deposition rate was regulated at around 0.2 Å/s with a quartz micro-balance for a total thickness of approximately 50 nm. The thin layers grown on the substrates at room temperature result clearly sub-oxidized, which turns out to be positive for their hole-selective behaviour [11]. These samples were used to characterize the ablation process with all the laser-sources specified in table 1.

Additionally, a similar set of samples of the three different metal oxides were processed to fabricate complete diodes. These rectifying devices were used to study the viability of a laser patterning process. In these samples the rear side was coated by a stack of thin intrinsic (4 nm) and heavily n-doped (15 nm) amorphous silicon layers, followed by a thick (500 nm) aluminium electrode. Such a standard heterojunction ensures a rear electron contact of excellent quality. As a front electrode we evaporated a thin nickel layer (10 nm) followed by a thicker aluminium capping (200 nm). The high work function of nickel preserves the hole-selectivity of the TMO layer, but an aluminium capping is needed for durability during the electrical measurements. A shadow mask was used during the evaporation of the front metallic contact, which defined test diodes with diameters ranging between 1 and 3 mm. The electrical characteristics were measured by means of a high-precision Keithley 2601B Source-Meter.

2.3. Measurements and characterization techniques

The morphological characterization of the samples was performed using a confocal microscope (Leica Sensofar DCM3D). The 3D images and profiles allowed a very precise measure of the film removal and the presence of substrate damage.

A way to compare the different processes, and a tool to select the more adequate laser system for the removal of the oxide, is the measure of the different fluence thresholds characteristic of the process: superficial damage of the oxide film, complete film removal, and presence of substrate damage. To determine the fluence thresholds, the oxide surface is irradiated with single laser pulses with different pulse energy, *Ep*, leading to marks and craters of different diameter. From the expression of the spatial fluence distribution of a Gaussian beam, it is possible to obtain a logarithmic relation between the diameter D of a mark or crater made in a material by a laser pulse, and the laser pulse peak fluence, ϕ_0:

$$D^2 = 2 \cdot w_0^2 ln\left[\frac{\phi_0}{\phi_{th}}\right] (1)$$

As f_0 is directly correlated with *Ep*, the laser beam radius can be obtained from the slope of that relation, and the ablation threshold fluence by subsequent back-extrapolation of the squared diameter to zero. This method, originally used to measure the fluence thresholds of 532 nm, ps pulses on crystalline silicon [32], has been successfully applied with different materials and applications, specifically for the removal of thin films [36].

This method allows the calculation of the process parametric window for each oxide and laser system, defined as the difference between the fluence thresholds of film removal and substrate damage.

From the results obtained in the process parameterization, the most suitable laser source was selected. A speed and repetition frequency parameterization were performed on all three oxides - WO_x, VO_x and MoO_x- to ensure that the overlap between pulses removes the oxide layer without damaging the silicon substrate. Finally, as a proof of concept, diodes based on these TMO/Si structures were laser-scribed. Their electrical characteristics were compared before and after laser insulation to check the quality of the process.

3. Results and discussion

3.1. Ablation thresholds

All the oxides studied here showed a similar behaviour: Nanosecond pulses at 355 nm and 532 nm generate craters with a better morphology, a clean edge. On the other hand, irradiation at 1064 nm generates more thermal affection. Picosecond pulses, due of the higher beam radius, induced a wider and more visible heat affected zone in the oxides surface. The dependence of the crater morphology on the laser wavelength and pulse duration has been observed in metals, semiconductors and polymers [16] [26] [27] [30]. Figure 1 includes a crater with good morphology (top image), showing a clean crater bottom and a well-defined crater edge, and another one (bottom image) with rough crater edges and a large affected area.

WO_x- 355 nm ns-pulsed (Ep ~ 8 µJ)

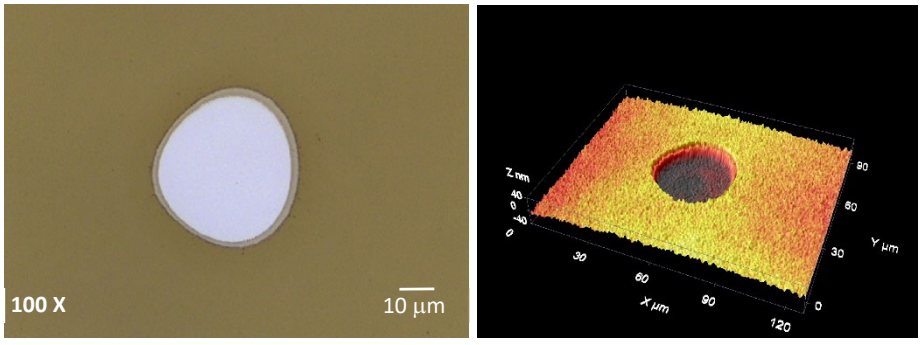

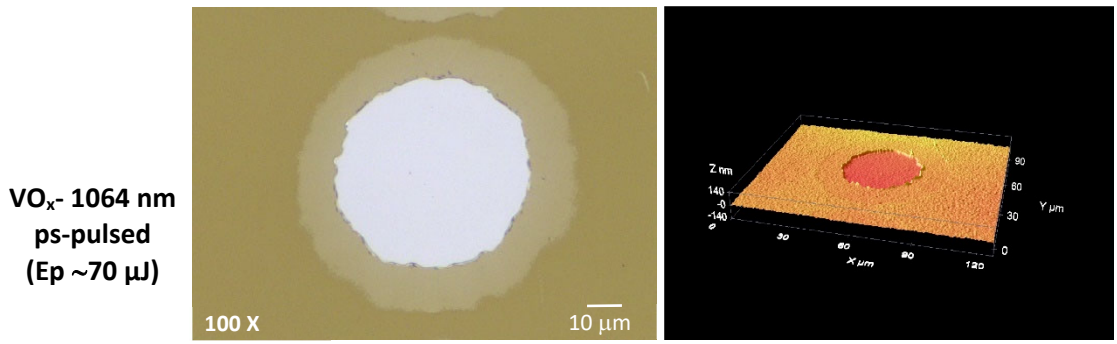

Figure 1. Confocal microscope images (left) and topography (right) of craters with good morphology at 355 nm for the WO_x at 8 µJ in nanoseconds pulses (top) and bad morphology at 1064 nm for VO_x at 70 µJ (bottom) in picoseconds pulses.

To illustrate the effect of the ns pulses, Figure 2 shows confocal microscopy images of 532 nm ns pulses in the MoO_x sample at different pulse energy. As it can be seen, as the pulse energy increases the damaged area grows and different effects on the material appear: an initial affectation on the oxide surface, which leads to the complete removal of the oxide layer and, for higher fluences, the damage of the silicon wafer. This fact allows defining three different regions in the ablated area. First, the outermost ring (black line in the right image of Figure 2) corresponds to the edge of the region in the oxide layer. The central ring (red line) corresponds to the removal of oxide layer. Finally, the inner ring (blue line) corresponds to the substrate damage where the depths are higher than the deposited film (>50 nm), as it can be seen in the crater profile.

When using picosecond pulses, for 532 nm no damage is observed on the surface of the oxide layer before it is totally removed. Therefore, we have considered both the oxide film damage threshold and the total removal threshold as the same value. Finally, when using 1064 nm no damage was detected on the silicon substrate for the studied pulse fluences.

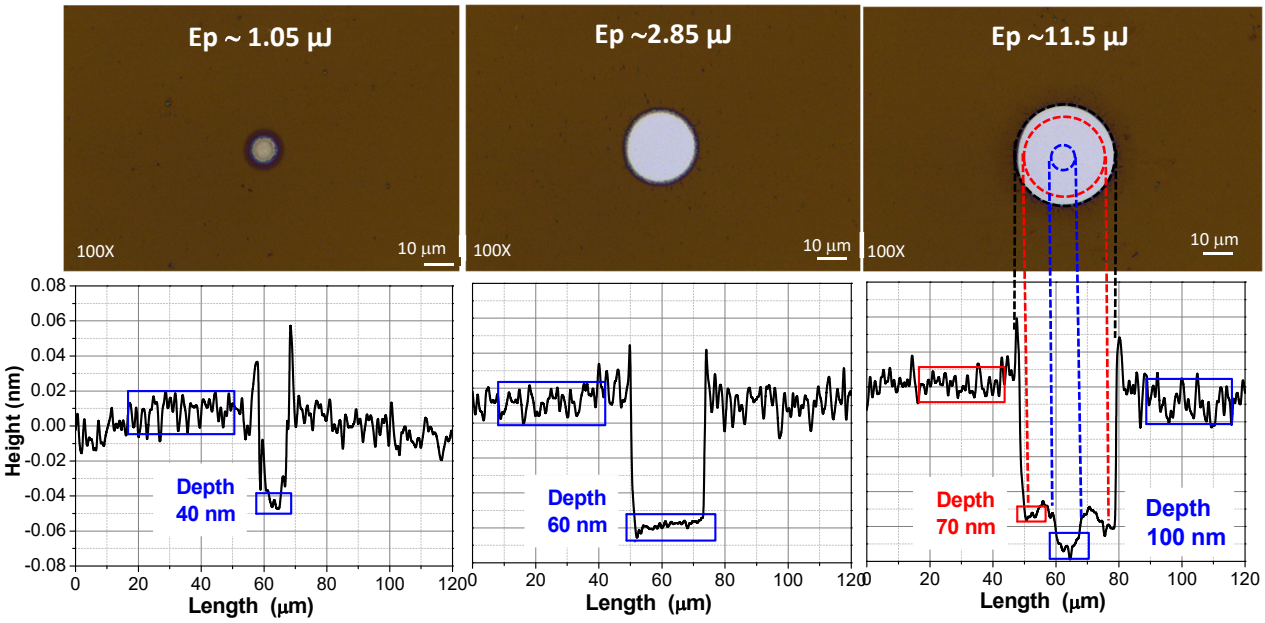

Figure 2. Confocal images and profiles of a typical laser ablation spot of oxide films at different energies per pulse. In this example, MoO_x is the transition metal oxide film. The laser source was emitting at 532 nm in ns-pulsed regime.

Figure 3 shows a graphical example of the relation between the squared of the crater diameter (D^2) and the logarithm of the applied Ep (left image) and the maximum laser pulse fluence (ϕ_0) (right image). A well-defined logarithmic dependence in a semi-log plot has been observed for all samples, allowing the calculation of the beam radius (ω_0). As expected, for each laser source, the obtained ω_0 values are almost independent of the studied oxide. The mean value of the

different ω_0 values obtained for the three oxides has been used for the fluence calculations. For the nanosecond lasers, the obtained beam radius (ω_0) values are 18.7 ± 0.7 µm, 14.2 ± 0.8 µm and 20.6 ± 0.1 µm for 355 nm, 532 nm, and 1064 nm wavelength, respectively. For the picosecond laser sources the obtained values are 33.1 ± 0.5 µm (at 355 nm), 42.2 ± 0.8 µm (at 532 nm), and 62 ± 1 µm (at 1064 nm).

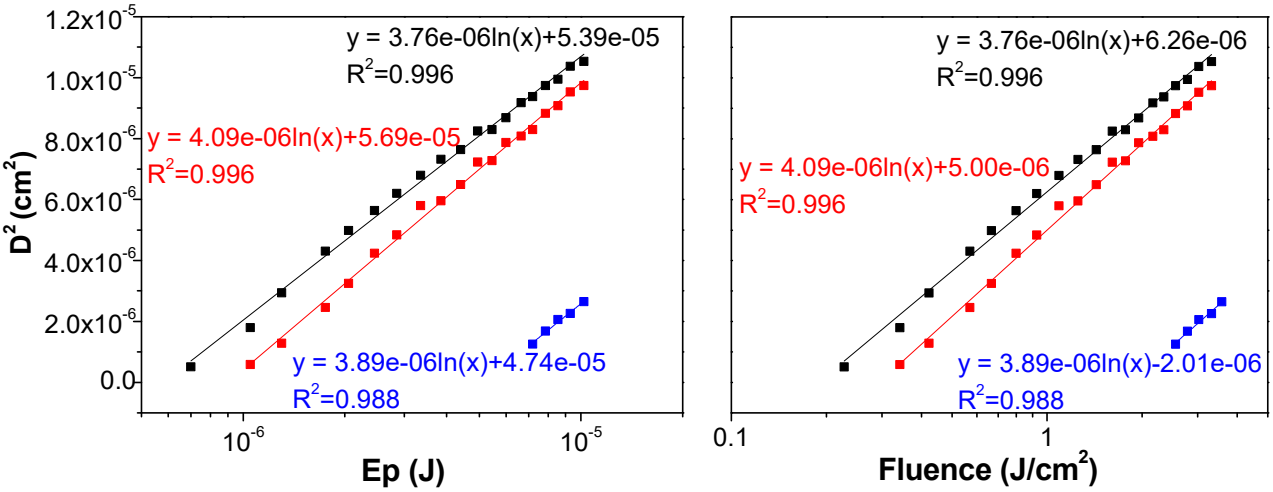

Figure 3. Squared diameter of laser-induced damage of MoOx films plotted versus applied pulse energy (left) and maximum pulse fluence (right). In this experiment, the laser source was emitting at 532 nm in ns-pulsed regime. (Black line -damage in the oxide film-, red line -total removal of the film- and blue line -substrate damage-).

The damage thresholds values for nano and picosecond pulsed lasers are gathered in Table 2.

Table 2. Damage threshold fluence for different oxides in ns and ps pulsed laser sources at 355nm, 532 nm and 1064 nm.

Oxides	ϕ_{th} (J/cm^2)								
	355 nm			532 nm			1064 nm		
	ns-pulsed								
	ϕ oxide damage	ϕ oxide removal	ϕ substrate damage	ϕ oxide damage	ϕ oxide removal	ϕ substrate damage	ϕ oxide damage	ϕ oxide removal	ϕ substrate damage
WO_x	0.12	0.17	1.87	0.28	0.31	1.98	4.27	4.93	10.36
VO_x	0.09	0.13	2.65	0.19	0.43	1.59	4.76	5.39	9.53
MoO_x	0.11	0.16	2.00	0.19	0.29	1.72	3.76	4.57	9.33
	ps-pulsed								
WO_x	0.05	0.09	0.64	0.19	0.19	0.19	0.65	0.65	>1.48
VO_x	0.02	0.04	0.58	0.14	0.14	>2.00	0.53	0.73	>1.48
MoO_x	0.04	0.06	0.45	0.17	0.17	0.38	0.40	0.51	>1.48

Figure 4 illustrates the threshold fluence, ϕ_{th}, obtained with each laser for the three oxides.

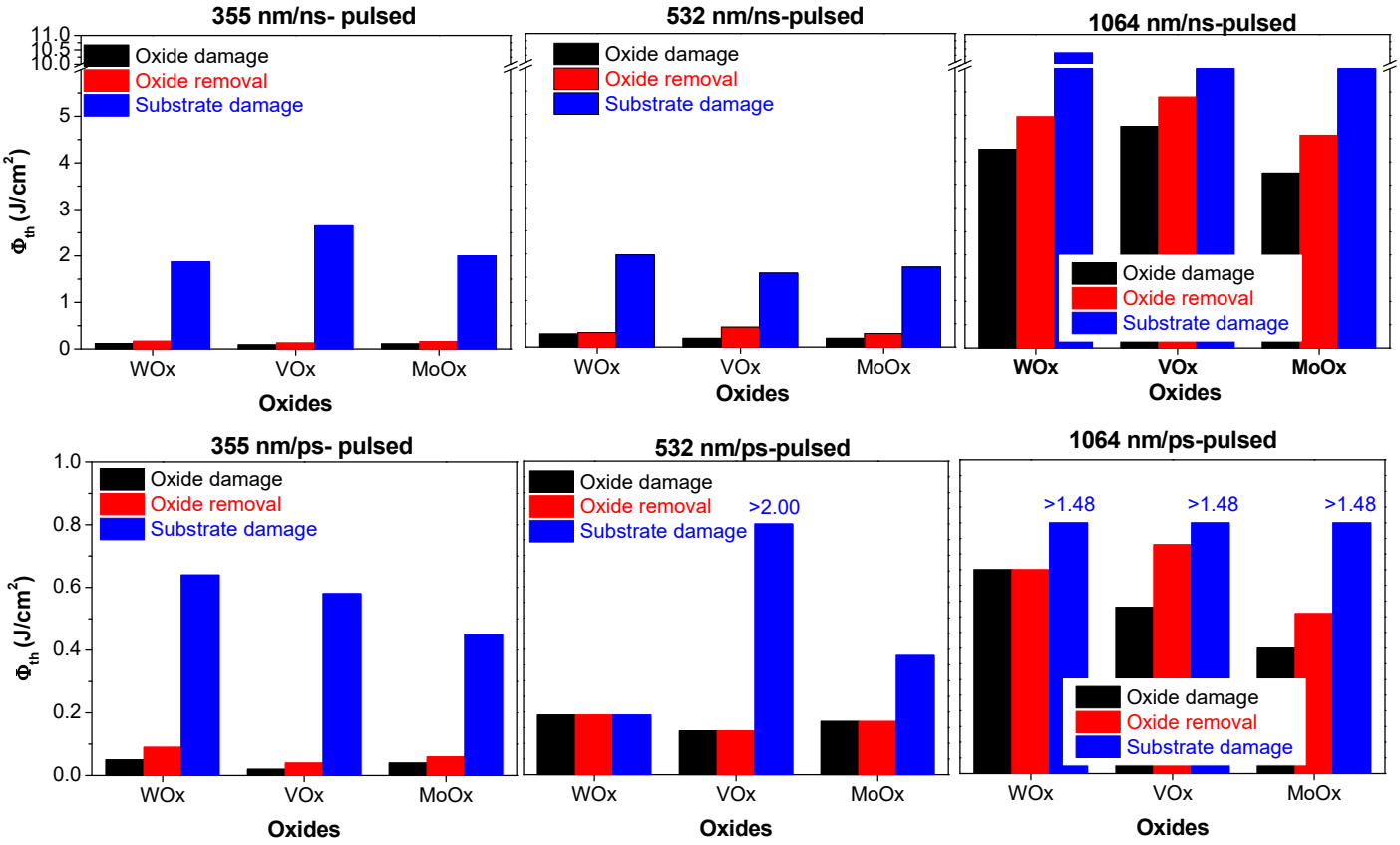

Figure 4. Threshold fluence for the three oxides studied in this work: nanosecond (top) and picosecond (bottom) pulses at 355 nm (left), 532 nm (centre), and 1064 nm (right). Please note the different scale for ns and ps experiments.

Working with nanosecond pulses (top row in Figure 4), a given wavelength leads to very similar threshold fluence to remove any of the three different oxides (red columns in Figure 4). The corresponding average values are respectively: 0.15 ± 0.02 J/cm^2 for 355 nm, 0.34 ± 0.08 J/cm^2 for 532 nm and 4.9 ± 0.4 J/cm^2 for 1064 nm. The ablation threshold obtained at 1064 nm is more than one order of magnitude higher than with the other wavelengths. This effect probably comes from the lower absorptivity of the material at this wavelength and, to a lesser extent, because of the longer pulse duration (120 ns at 1064 nm versus 12 ns and 15 ns at 355 nm and 532 nm, respectively).

As commented before, in the picosecond regime and depending on the oxide film three different rings are not observed. Therefore, the damage threshold has been assumed to correspond with the layer removal threshold. In the case of picosecond pulses, the average threshold fluences obtained for the oxide removal are 0.06 ± 0.02 J/cm^2 for 355 nm, 0.16 ± 0.02 J/cm^2 for 532 nm and 0.6 ± 0.1 J/cm^2 for 1064 nm. As expected, these values are lower than the threshold values obtained in nanosecond regime due to the shorter duration of the pulses -8ps in all wavelengths-. Longer laser pulses allow a higher thermal diffusion, with a deeper propagation of the thermal wave into the sample, demanding more energy to remove the oxide layer [30].

Table 3 summarizes the parametric window for the three oxides studied in this work for each wavelength of ns and ps laser pulses. It is observed that for ns-pulses the parametric window between oxide removal and substrate damage for a given wavelength is very similar for the three oxides, around 2.0 J/cm^2 for 355 nm, 1.5 J/cm^2 for 532 nm, and 5.5 J/cm^2 for 1064 nm. On the other hand, with ps-pulses the three wavelengths can be used to remove the three oxides. However, we found parametric windows for all the oxides only at 355 nm, and for MoO_x at 532 nm. In the case of 1064 nm pulses, the maximum pulse fluence values used did not produce

damage in the silicon substrate. The substrate damage threshold was over the fluence values used throughout the complete experiment. Note that this happened also when irradiating the VOx films with 532 nm. Finally, for WO_x with ps pulses at 532 nm the substrate is damaged at the same time that the oxide is removed. Then, in that case there is no parametric window between oxide film removal and substrate damage.

In summary, excluding WO_x when using 532 nm picosecond pulses, all laser systems make possible the removal of the VO_x, WO_x and MoO_x films with no damage to the substrate. With ns pulses the oxide layers show a similar behaviour for a given wavelength, with higher threshold values at 1064 nm. With ps pulses, slightly lower fluences are needed to remove the oxide films, probably because the shorter duration of the pulses prevents thermal diffusion into the substrate.

Table 3. Parametric windows of oxide removal process for ns and ps pulses at 355 nm, 532 nm and 1064 nm.

		Parametric Window (J/cm²)		
		355 nm	**532 nm**	**1064 nm**
WO_x	**ns-pulsed**	0.17 – 1.87	0.31 – 1.98	4.93 – 10.36
	ps-pulsed	0.09 – 0.64	0.19 – 0.19	0.65 – > 1.48
VO_x	**ns-pulsed**	0.13 – 2.65	0.43 – 1.59	5.39 – 9.53
	ps-pulsed	0.04 – 0.58	0.14 – >2.00	0.73 – > 1.48
MoO_x	**ns-pulsed**	0.16 – 2.00	0.29 – 1.72	4.57 – 9.33
	ps-pulsed	0.06 – 0.45	0.17 – 0.38	0.51 – > 1.48

The threshold fluence for the oxide removal increases with the wavelength in the three oxides (red column in figure 4). This is probably due to the longer optical penetration depth of the radiation that reduces the energy absorption in the film at higher wavelengths. Consequently, a shorter wavelength, i.e., UV radiation, results in a lower fluence needed to damage the film. This effect has been observed recently for the ablation of PECVD SiNx layers on silicon with ps-laser pulses at different wavelengths [29] [38]. On the other hand, the different pulse duration for a given wavelength could also influence the measured threshold fluences.

3.2. Diode electric isolation

Finally, we investigated the viability of using the optimized laser ablation steps to pattern devices with these oxides. For that purpose, we fabricated diodes on n-type c-Si with a reference ohmic contact of doped amorphous silicon on the rear side (cathode). On the front side, the three different oxides were used as hole-selective electrodes with circular aluminium contacts (anode). For these processes, it was decided to use the laser source emitting at 532 nm in ns regime. This system led to craters with good morphology and a quite wide parametric window. To avoid damage in the silicon substrate we made a parametrization of the isolation process focused on the overlap between laser pulses. For the three oxides -WO_x, VO_x and MoO_x- the ablated layer is around 20-30 nm, so the silicon substrate is not damaged in any case. Figure 5 shows a diode of MoO_x with diameter 1.5 mm that has been isolated by laser ablation at 0.25 mm of the contact edge. The homogeneity and continuity of the process without damaging the substrate is observed.

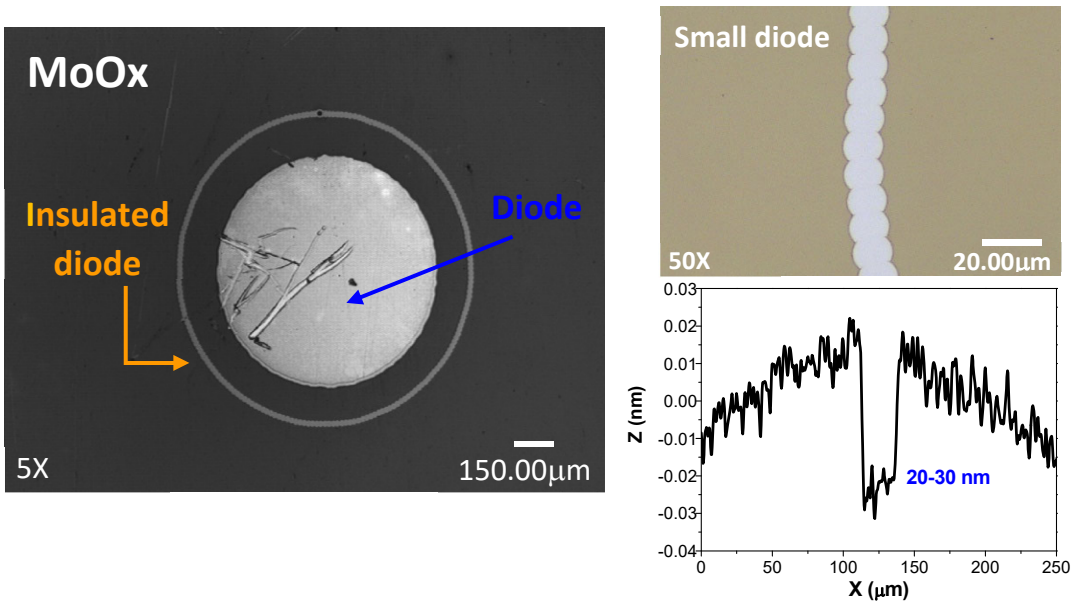

Figure 5. Top microscopy image of a MoO_x diode isolated by laser ablation (left). Confocal image and profile of a laser ablated spot on the MoO_x film (right). The laser used was emitting at 532 nm (VIS) in ns-pulsed regime.

Figure 6 shows the electrical characteristics of diodes with the three different oxides before and after the laser insulation process. It is observed a remarkable improvement in all the cases, with a reduction of the reverse current density by two orders of magnitude. It has been reported that the high work function of transition metal oxides induces an inversion layer at the c-Si surface [37]. This results in a leakage current that extends in the region surrounding the metallic contact. Such parasitic effect can be minimized by insulating the active area by laser ablation, as it is shown in figure 5 (left). The methodology developed here could be applied to define more complex patterns, such as interdigitated contacts or planar device architectures. Note that the properties of transition metal oxides may be altered by solvents or in thermal steps used for conventional lithography.

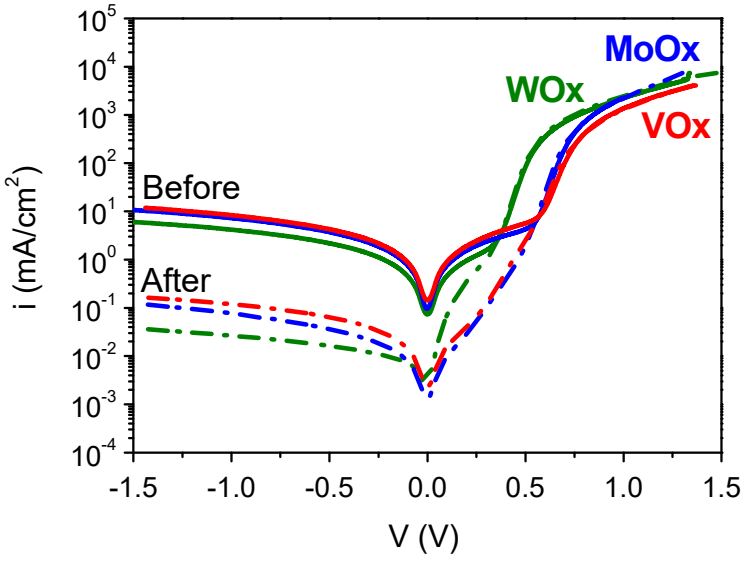

Figure 6. Dark JV curves of WO_x, VO_x and MoO_x diodes before and after isolation.

4. Conclusions

In summary, we present a complete study of laser ablation for three different oxides -WO_x, VO_x, and MoO_x deposited by means of evaporation on silicon - using 355 nm, 532 nm, and 1064 nm wavelengths, with pulse duration in the nanosecond and picosecond regimes. These oxides have interesting properties as selective contact layers for novel semiconductor devices.

The behaviour of the three oxides under laser irradiation in different conditions is quite similar, both concerning the wavelength and pulse width influence on the ablation process. Also, we observed that the longer wavelength (1064 nm) induces rougher crater edges with re-solidified material, while the shortest wavelength (355 nm) produces a neat edge. Furthermore, taking into account the parametric windows of each case, the best option to ablate the oxide layers without affecting the substrate is to use laser sources in nanoseconds regime where the set of parameter values that lead to a good oxide film removal is greater. Also, the best choice for the ablation is to use short wavelengths, UV (355 nm) and VIS (532 nm), due to the lower thermal effects obtained at the crater edges in both cases. As 532 nm pulses lead to a cleaner crater bottom, we use this approach to isolate diodes fabricated by the evaporation of round metallic contacts on the oxide surface. We obtained homogeneous and continuous laser grooves, and the diode isolation reduces up to two orders of magnitude the diodes reverse current density for the three different oxides.

5. Acknowledgements

Partial financial support for this work has been provided by the Spanish Ministry of Science and Innovation under the projects CHENOC (ENE2016-78933-C4-1-R and ENE2016-78933-C4-4-R) and SCALED (PID2019-109215RB-C41 and PID2019-109215RB-C44).

6. References

[1] M. Taguchi *et al.*, “24.7% Record Efficiency HIT Solar Cell on Thin Silicon Wafer,” *IEEE J. Photovoltaics*, vol. 4, no. 1, pp. 96–99, Jan. 2014.

[2] A. Descoeudres *et al.*, “Improved amorphous/crystalline silicon interface passivation by hydrogen plasma treatment,” *Appl. Phys. Lett.*, vol. 99, no. 12, Sep. 2011.

[3] Y. Hamakawa, K. Fujimoto, K. Okuda, Y. Kashima, S. Nonomura, and H. Okamoto, “New types of high efficiency solar cells based on a-Si,” *Appl. Phys. Lett.*, vol. 43, no. 7, pp. 644–646, 1983.

[4] S. DeWolf, A. Descoeudres, Z. C. Holman, and C. Ballif, “High-efficiency silicon heterojunction solar cells: A review,” *Green*, vol. 2, no. 1. Walter de Gruyter GmbH, pp. 7–24, 2012.

[5] F. Feldmann, M. Bivour, C. Reichel, M. Hermle, and S. W. Glunz, “Passivated rear contacts for high-efficiency n-type Si solar cells providing high interface passivation quality and excellent transport characteristics,” *Sol. Energy Mater. Sol. Cells*, vol. 120, no. PART A, pp. 270–274, 2014.

[6] Institute of Electrical and Electronics Engineers, F. IEEE Photovoltaic Specialist Conference 42 2015.06.14-19 Tampa, F. IEEE Photovoltaic Specialists Conference 42 2015.06.14-19 Tampa, and F. PVSC 42 2015.06.14-19 Tampa, *2015 IEEE 42nd Photovoltaic Specialist Conference (PVSC) 14-19 June 2015, New Orleans, LA*. .

[7] J. Meyer, S. Hamwi, M. Kröger, W. Kowalsky, T. Riedl, and A. Kahn, “Transition metal oxides for organic electronics: Energetics, device physics and applications,” *Advanced Materials*, vol. 24, no. 40. pp. 5408–5427, Oct-2012.

[8] C. Battaglia *et al.*, “Silicon heterojunction solar cell with passivated hole selective MoO x contact,” *Appl. Phys. Lett.*, vol. 104, no. 11, p. 113902, Mar. 2014.

[9] F. Feldmann *et al.*, “High and Low Work Function Materials for Passivated Contacts,” *Energy Procedia*, vol. 77, pp. 263–270, Aug. 2015.

[10] J. P. S. S. S. B. M. W. M. M. E. K. J. G. S. D. W. and C. B. B. Demaurex, “ Photovoltaics, IEEE Journal of 4 (2014) 1387,” *Photovoltaics, IEEE J.*, vol. 4, 2014.

[11] L. G. Gerling *et al.*, “Transition metal oxides as hole-selective contacts in silicon heterojunctions solar cells,” *Sol. Energy Mater. Sol. Cells*, vol. 3, pp. 109–115, 2016.

[12] C. Battaglia *et al.*, “Hole Selective MoOx Contact for Silicon Solar Cells.,” *Nano Lett.*, vol. 14, no. 2, pp. 967–71, Feb. 2014.

[13] J. Hermann *et al.*, “Selective ablation of thin films with short and ultrashort laser pulses,” *Appl. Surf. Sci.*, vol. 252, no. 13 SPEC. ISS., pp. 4814–4818, 2006.

[14] S. Zoppel, H. Huber, and G. A. Reider, “Selective ablation of thin Mo and TCO films with femtosecond laser pulses for structuring thin film solar cells,” *Appl. Phys. A Mater. Sci. Process.*, vol. 89, no. 1, pp. 161–163, Oct. 2007.

[15] D. Canteli *et al.*, “Picosecond-laser structuring of amorphous-silicon thin-film solar modules,” *Appl. Phys. A Mater. Sci. Process.*, vol. 112, no. 3, pp. 695–700, Sep. 2013.

[16] S. Lauzurica, J. J. García-Ballesteros, M. Colina, I. Sánchez-Aniorte, and C. Molpeceres, “Selective ablation with UV lasers of a-Si:H thin film solar cells in direct scribing configuration,” in *Applied Surface Science*, 2011, vol. 257, no. 12, pp. 5230–5236.

[17] D. Canteli, I. Torres, J. J. García-Ballesteros, J. Cárabe, C. Molpeceres, and J. J. Gandía, “Characterization of direct- and back-scribing laser patterning of SnO<inf>2</inf>:F for a-Si:H PV module fabrication,” *Appl. Surf. Sci.*, vol. 271, 2013.

[18] J. J. García-Ballesteros *et al.*, “Comparative analysis of laser generated P2 processes for a-Si:H modules and their electrical influence on the final device,” in *Physics Procedia*, 2013, vol. 41.

[19] J. J. J. García-Ballesteros, I. Torres, S. Lauzurica, D. Canteli, J. J. J. Gandía, and C. Molpeceres, “Influence of laser scribing in the electrical properties of a-Si:H thin film photovoltaic modules,” *Sol. Energy Mater. Sol. Cells*, vol. 95, no. 3, pp. 986–991, Mar. 2011.

[20] T. D. A. O. N. N. D. V. D. Muñoz, “Progress on high efficiency standard and interdigitated back contact silicon heterojunction solar cells ,” *26th Eur. Photovolt. Sol. Energy Conf. Exhib.*, 2011.

[21] J. Liu, Y. Yao, S. Xiao, and X. Gu, “Review of status developments of high-efficiency crystalline silicon solar cells,” *Journal of Physics D: Applied Physics*. 2018.

[22] M. Weizman *et al.*, “Rear-side All-by-Laser Point-contact Scheme for liquid-phase-crystallized silicon on glass solar cells,” *Sol. Energy Mater. Sol. Cells*, vol. 137, pp. 280–286, 2015.

[23] S. Rung, A. Christiansen, and R. Hellmann, “Influence of film thickness on laser ablation threshold of transparent conducting oxide thin-films,” *Appl. Surf. Sci.*, vol. 305, pp. 347–351, 2014.

[24] G. Heise, M. Domke, J. Konrad, S. Sarrach, J. Sotrop, and H. P. Huber, “Laser lift-off initiated by direct induced ablation of different metal thin films with ultra-short laser pulses,” *J. Phys. D. Appl. Phys.*, vol. 45, no. 31, 2012.

[25] “sundaram2002 Inducing and probing non-thermal transitions in semiconductors using femtosecond laser pulses.”

[26] S. Hermann, N. P. Harder, R. Brendel, D. Herzog, and H. Haferkamp, “Picosecond laser ablation of SiO2layers on silicon substrates,” *Appl. Phys. A Mater. Sci. Process.*, vol. 99, no. 1, pp. 151–158, 2010.

[27] L. Torrisi, A. Borrielli, and D. Margarone, “Study on the ablation threshold induced by pulsed lasers at different wavelengths,” *Nucl. Instruments Methods Phys. Res. Sect. B Beam Interact. with Mater. Atoms*, vol. 255, no. 2, pp. 373–379, 2007.

[28] C. Molpeceres, S. Lauzurica, J. L. Ocãa, J. J. Gandía, L. Urbina, and J. Cárabe, “Microprocessing of ITO and a-Si thin films using ns laser sources,” *J. Micromechanics Microengineering*, vol. 15, no. 6, pp. 1271–1278, 2005.

[29] G. Heinrich, M. Bähr, K. Stolberg, T. Wütherich, M. Leonhardt, and A. Lawerenz, “Investigation of ablation mechanisms for selective laser ablation of silicon nitride layers,” *Energy Procedia*, vol. 8, pp. 592–597, 2011.

[30] B. N. Chichkov, C. Momma, S. Nolte, F. Von Alvensleben, and A. Tünnermann, “Femtosecond, picosecond and nanosecond laser ablation of solids,” *Appl. Phys. A Mater. Sci. Process.*, 1996.

[31] J. Hermann *et al.*, “Comparative investigation of solar cell thin film processing using nanosecond and femtosecond lasers,” *J. Phys. D. Appl. Phys.*, vol. 39, no. 3, pp. 453–460, 2006.

[32] J. M. Liu, “Simple technique for measurements of pulsed Gaussian-beam spot sizes,” *Opt. Lett.*, vol. 7, no. 5, p. 196, 1982.

[33] S. Xiao, E. L. Gurevich, and A. Ostendorf, “Incubation effect and its influence on laser patterning of ITO thin film,” *Appl. Phys. A Mater. Sci. Process.*, vol. 107, no. 2, pp. 333–338, 2012.

[34] J. Bonse, J. M. Wrobel, J. Krüger, and W. Kautek, “Ultrashort-pulse laser ablation of indium phosphide in air,” *Appl. Phys. A Mater. Sci. Process.*, vol. 72, no. 1, pp. 89–94, 2001.

[35] G. Heise *et al.*, “Investigation of the ablation of zinc oxide thin films on copper-indium-selenide layers by ps laser pulses,” *Appl. Phys. A Mater. Sci. Process.*, vol. 104, no. 1, pp. 387–393, 2011.

[36] G. Heise, M. Englmaier, C. Hellwig, T. Kuznicki, S. Sarrach, and H. P. Huber, “Laser ablation of thin molybdenum films on transparent substrates at low fluences,” *Appl. Phys. A Mater. Sci. Process.*, vol. 102, no. 1, pp. 173–178, 2011.

[37] J. Bullock, A. Cuevas, T. Allen, and C. Battaglia, “Molybdenum oxide MoO x : A versatile hole contact for silicon solar cells,” *Appl. Phys. Lett.*, vol. 105, no. 23, p. 232109, Dec. 2014.